Probing Jovian Decametric Emission with the Long Wavelength Array Station 1

T. E. Clarke[1], C. A. Higgins[2], Jinhie Skarda[3], Kazumasa Imai[4], Masafumi Imai[5], Francisco Reyes[6], Jim Thieman[7], Ted Jaeger[8], Henrique Schmitt[1] Nagini Paravastu Dalal[9], Jayce Dowell[10], S. W. Ellingson[11], Brian Hicks[1], Frank Schinzel[10], G. B. Taylor[10]

arXiv:1412.7237v1 [astro-ph.EP] 23 Dec 2014

Abstract. New observations of Jupiter's decametric radio emissions have been made with the Long Wavelength Array Station 1 (LWA1) which is capable of making high quality observations as low as 11 MHz. Full Stokes parameters were determined for bandwidths of 16 MHz. Here we present the first LWA1 results for the study of six Io-related events at temporal resolutions as fine as 0.25 ms. LWA1 data show excellent spectral detail in Jovian DAM such as simultaneous left hand circular (LHC) and right hand circular (RHC) polarized Io-related arcs and source envelopes, modulation lane features, S-bursts structures, narrow band N-events, and interactions between S-bursts and N-events. The sensitivity of the LWA1 combined with the low radio frequency interference environment allow us to trace the start of the LHC Io-C source region to much earlier CML III than typically found in the literature. We find the Io-C starts as early as CML III = 230° at frequencies near 11 MHz. This early start of the Io-C emission may be valuable for refining models of the emission mechanism. We also detect modulation lane structures that appear continuous across LHC and RHC emissions, suggesting that both polarizations may originate from the same hemisphere of Jupiter. We present a study of rare S-bursts detected during an Io-D event and show drift rates are consistent with those from other Io-related sources. Finally, S-N burst events are seen in high spectral and temporal resolution and our data strongly support the co-spatial origins of these events.

1. Introduction

Strong bursts of decametric radio emission below 40 MHz were identified by Burke & Franklin [1955] as originating from Jupiter. The emission in the decametric range (referred to as DAM range hereafter) occurs from 3 MHz to 39.5 MHz, although specific Io-related DAM arcs have been seen at frequencies below 2 MHz [Zarka et al., 2001; Queinnec & Zarka, 1998; Alexander et al., 1981]. Jovian DAM has a peak of the spectral power at a frequency of about 10 MHz, and average fluxes of 10 MJy[1], as well as S-bursts that can be 100 times stronger [Zarka, 1998]. The lower-limit on observations from ground-based observatories is generally above 5 to 10 MHz due to attenuation by the Earth's ionosphere.

From ground-based and space-based observations, it has been long known that much of the Jupiter DAM emission is influenced by the satellite Io [Bigg, 1964], and that some emissions not related to Io have been correlated with solar wind parameters [Barrow et al., 1986; Hess et al., 2012]. For a review see Carr et al. [1983]. These coherent emissions are thought to be the result of instabilities near the local electron cyclotron frequency, called the cyclotron maser instability (CMI) mechanism [Treumann, 2006; Zarka, 1998; Wu & Lee, 1979]. The CMI emission is beamed in a hollow cone with thickness of a few degrees [Kaiser et al., 2000] which has a large half-angle of 60° to 90° relative to the local magnetic field direction [Hess et al., 2008; Queinnec & Zarka, 1998; Dulk, 1967]. The DAM emission is observed at Earth when the edge of the emission cone sweeps over the observer. General properties of the DAM emission include 1) high brightness temperatures, $> 10^{15}$ K, 2) emission at frequencies near the X-mode cutoff which is close to the local electron cyclotron frequency from both northern and southern hemisphere emission regions, and 3) 100% circular or elliptical polarization [Clarke et al., 2004].

The Io-controlled Jovian emission regions are designated Io-A and Io-B for the primarily right hand circular (RHC) emission sources in the northern hemisphere while the predominantly left hand circular (LHC) sources in the southern hemisphere are designated Io-C and Io-D. The handedness of the polarized emission is set by the direction of propagation of the emission relative to the local magnetic field direction as seen by the observer [Zarka, 1988; Thieman & Smith, 1979]. These Io-related emission regions are defined

[1]Naval Research Laboratory, Code 7200, Washington, DC, USA.
[2]Department of Physics and Astronomy, Middle Tennessee State University, Murfreesboro, TN, USA.
[3]Department of Electrical Engineering, Stanford University, Stanford, CA, USA.
[4]Department of Electrical Engineering and Information Science, Kochi National College of Technology, Kochi, Japan.
[5]Department of Geophysics, Kyoto University, Japan
[6]Department of Astronomy, University of Florida, Gainesville, FL, USA.
[7]NASA/GSFC, Code 6901, Greenbelt, MD, USA.
[8]Johns Hopkins University Applied Physics Laboratory, Laurel, MD, USA.
[9]Work done as ASEEE at NRL, Code 7200, Washington, DC, USA.
[10]Department of Physics and Astronomy, University of New Mexico, Albuquerque, NM 87131, USA.
[11]Bradley Department of Electrical & Computer Engineering, Virginia Tech, Blacksburg, VA 24060, USA.

Copyright 2014 by the American Geophysical Union.
0148-0227/14/$9.00

Table 1. LWA1 Array Comparison with other Decameter Telescopes used for Jovian Study

Name	Dipole Type Type	Number of Dipoles x Polarizations	Freq (MHz)	Sensitivity[1], BW mJy, MHz	Reference
LWA1	Bowtie	256 x 2	10-88	17, 16	1
Nançay Decameter Array	Conical Log Spiral	72 x 2	10-120	1670, 1	2
UTR-2	Cylinder	(1440 + 600) x 1	8-30	10000, 3	3
LOFAR LBA Station	Wire	48 x 2	10-90	40, 16	4

[1] Zenith sensitivity at 20 MHz in 1 hr at listed bandwidth (BW). Values from Taylor et al. [2012] except NDA from Lecacheux et al. [1991].

References: 1. Ellingson et al. [2013], 2. Boischot et al. [1980], 3. Braude et al. [1978], 4. van Haarlem et al. [2013]

by their occurrence probability in the central meridian longitude (CML III) and Io-phase (ϕ_{Io}) plane [Carr et al., 1983].

There are many types of fine structures seen in Jovian decametric radio emission. Most of these structures have been seen by other ground-based and spacecraft observers [Zarka, 1998; Carr et al., 1983]. Common features include emission frequency envelopes that differ for Io and non-Io related events, as well as spectral arc structures that depend both on the frequency and the Io/non-Io source parameters [Hess et al., 2008; Carr et al., 1983]. Jupiter DAM emission can be further characterized as consisting of a set of long bursts (L-bursts) which last several minutes but have temporal substructure (few seconds) modulated by interplanetary scintillations, short milli-second bursts (S-bursts), as well as narrow band emission (N-events). While the L-bursts are modulated by scintillation, the S-bursts show modulation and both simple and complex structure that is intrinsic to the source regions [Arkypov & Rucker, 2009; Hess et al., 2007; Carr & Reyes, 1999; Carr et al., 1983]. The N-events have been observed since the 1960s and show widely varying bandwidths from 15 kHz to 200 kHz and have durations from seconds to many minutes [Riihimaa, 1985; Carr et al., 1983]. The N-events also show complex structure such as splitting and interactions with S-bursts, called S-N events, [Oya et al., 2002; Riihimaa & Carr, 1981; Boischot et al., 1980] and are seen both with smooth and erratic frequency drift rates.

The basic envelope and arc structure of bursts comes from the rotating conical beam pattern and Alfvén wave propagation and reflection along Io's flux tube [Hess et al., 2008; Queinnec & Zarka, 1998]. L-bursts are from CMI emission occurring as trains of emission interrupted by modulations in Jupiter's Io plasma torus as well as interplanetary and terrestrial ionospheric scintillations [Carr et al., 1983]. S-bursts are CMI emission thought to be produced by 5 keV electrons accelerated along magnetic field lines connecting to Io [Hess et al., 2007; Zarka et al., 1996]. S-N event emissions are not well understood but they are believed to be interactions at the source between precipitating electrons and resonant emission regions [Oya et al., 2002; Carr et al., 1983].

There are also additional structures seen within the Jovian emission such as the modulation lanes first seen by Riihimaa [1968]. These lanes are seen as groupings of equally-spaced intensity variations running across multiple L-bursts. The modulation lanes are known to slope upward or downward in frequency and the typical separation of the lanes is of order 2 s. The modulations lanes can generally be traced over large frequency ranges of 5 to 10 MHz. The origin of these modulation lanes is not completely understood but one model, which fits well with the data, demonstrates that the lanes originate from an interference pattern generated by passage of the Jovian decametric emission through vertical plasma density fluctuations along magnetic field lines located near Io's orbit close to the longitude of the sub-Earth point [Imai et al., 1992]. This model is capable of yielding new and detailed information regarding the Jovian decametric sources and the environment near Io's orbit in which the interference-producing plasma structure is located.

Despite extensive study of Jovian decametric emission since its discovery in 1955, there are still many open issues such as the nature of the emission and particle acceleration mechanism(s), the three dimensional structure and location of the DAM emission cones, the local plasma densities in the satellite flux tubes, processes influenced by the solar wind and by Io, and the physical processes responsible for the fine spectral signatures (modulation lanes, S-bursts, N-events, etc.). In this paper we present an overview of our Jovian observing campaign using the newly developed Long Wavelength Array Station One (LWA1). These observations agree well with studies from the literature, and allow us to extend our understanding of the Jovian emission by showing the early start of Io-C emission at low frequencies (Section 4.1) as well as revealing the structure of rare S-bursts seen during Io-D events (Section 5.3.2). These results show the power of the LWA1 instrument for Jovian research and may lead to refinements in our understanding of the Jovian emission processes.

2. Instrument: The Long Wavelength Array Station One

Observations of Jovian decametric emission were obtained using the first station of the Long Wavelength Array. LWA1 is a low frequency radio dipole array located in New Mexico near the National Radio Astronomy Observatory's Jansky Very Large Array. We summarize relevant instrumental parameters below and refer the reader to Ellingson et al. [2013] for a more complete description of the instrument.

LWA1 consists of 256 dual polarization antennas. Each antenna has an active-balun-preamp-filter design that gives 6 dB gain above the Galactic background over the bandwidth 20-80 MHz without increasing the overall noise of the system. The tuneable range of LWA1 is 10-88 MHz. Details of the "active" antenna system are presented in Hicks et al. [2012].

The outputs of the LWA1 antennas are digitized, delayed, and summed to form up to four independently pointed beams on the sky. Each beam has two fully independent frequency tunings with bandwidths that can be selected between roughly 0.2 MHz and 16 MHz. Each LWA1 beam provides dual orthogonal linear polarizations such that it is possible to reconstruct the full Stokes parameters for each tuning. LWA1 also operates with a transient buffer mode that digitizes each polarization from each antenna to provide all-sky imaging [Ellingson et al., 2013].

The system equivalent flux density (SEFD) of an array provides a measure of the combined sensitivity of the array and receiver system. SEFD can be thought of as the flux density of an unresolved radio source in the beam that doubles the measured system power relative to measurements without the source. The SEFD of the LWA1 is measured by Ellingson et al. [2013] as 16.1 kJy (single polarization) at 74.03 MHz using Cygnus A which is in a relatively bright part of the sky. Table II of Ellingson et al. [2013] reports the single polarization LWA1 SEFD for Cygnus A at 37.9, 28.8, and 20.5 MHz to be 21.5, 18.2, and 47.0 kJy. The SEFD measurement will decrease away from the Galactic

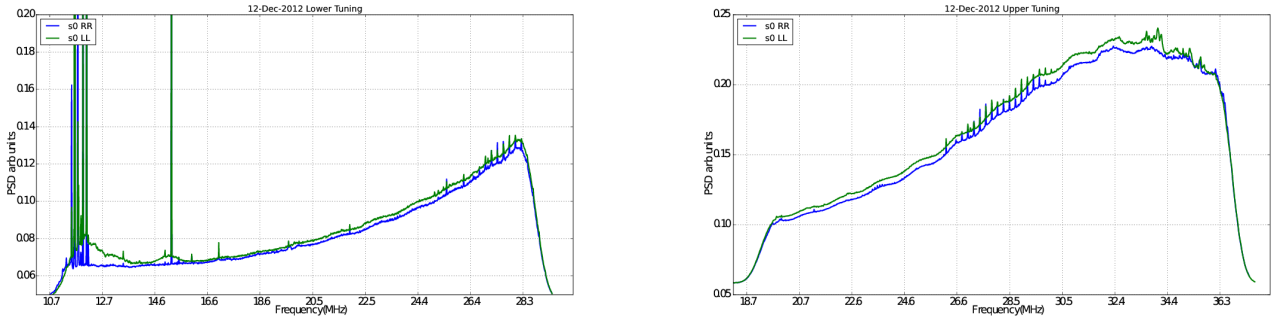

Figure 1. Top panel shows the LWA1 bandpass of the Jupiter beam for R and L polarizations (blue and green, respectively) for the lower tuning (ν_{center}=20 MHz). The bandpasses were made using 120 s of data during a non-bursting portion of the Jovian observing. There has been no removal of RFI. Bottom panel shows the bandpass at the same time for the upper tuning (ν_{center}=28 MHz).

plane and also depends inversely on elevation. The impact of source location and elevation can be seen in Figure 12 of the Ellingson et al. [2013] paper where measurements at several frequencies and zenith angles toward a variety of sources in and out of the Galactic plane are presented. The SEFD of the LOFAR low-band antennas (LBA) as shown in van Haarlem et al. [2013] at roughly 38 MHz is 32 kJy for the LBA outer core stations and 38 kJy for the LBA Inner core stations. At 30 MHz, the lowest measurements shown in van Haarlem et al. [2013], the LOFAR SEFD is roughly 38 kJy for both LBA inner and outer core stations. We note that comparable SEFD measurements are not available for the Nançay Decameter Array (NDA hereafter) and UTR-2 so it is not possible to compare them on a consistent (i.e. SEFD) basis with the LWA1. Taylor et al. [2012] compare the zenith sensitivity of low frequency instruments (except NDA) for 1 hour observations at typical bandwidths for the instruments in their Figure 2. In Table 1 we provide a comparison of dipole type, number of dipoles, number of polarizations, frequency coverage and Zenith sensitivity of several low frequency instruments typically used for Jovian decametric research. We use the numbers from Figure 2 of Taylor et al. [2012] and add the sensitivity of NDA from Lecacheux et al. [1991].

2.1. Jovian Program Observing Setup

Jovian decametric emission is confined to the lower half of the LWA1 frequency band below 40 MHz. Observation campaigns were undertaken mainly within the typical Jovian observing season when Jupiter is visible at night, although a few observations were also taken outside this season during daytime. The observing schedule was determined using the known Io-related burst probability distribution[2]. We mainly targeted long duration bursts (greater than 30 minutes) at high elevations where the burst probability passed through the highest probability regions.

The observations were all taken in wide bandwidth mode with a total observing bandwidth of 16 MHz. The majority of the observations were obtained with tunings centered at 20 and 28 MHz. These passbands contain significant overlap allowing us to cover the entire frequency range of 10.2 MHz to 37.8 MHz with the frequency range of 12 - 36 MHz having nominal sensitivity. Several of the Io-B events were observed at higher tunings of 22 and 30 MHz due to the generally higher peak frequency emission observed from these events, thus allowing nominal sensitivity over the 14 - 38 MHz range. In addition to the beam tracking Jupiter, we also used identical tunings for one to two off-beams which are used for data quality and instrumental bandpass analysis. These off-beams were centered on a range of targets including several well-established radio calibrators such as the supernova remnants Cas-A, and the Crab Nebula, as well as the extragalactic radio galaxy Cyg-A. Additional off-beam data was also obtained from the north celestial pole.

The LWA1 beam full width at half maximum near zenith ranges from 8.1° at 20 MHz to 5.8° at 30 MHz [Ellingson et al., 2013]. Although most bursts were targeted for high elevations, some bursts were tracked for very long times and reached low elevations of roughly 10°. At these elevations the LWA1 beam will be significantly elongated.

In this paper we present a subset of the LWA1 Jovian observations to provide on overview of the capabilities of the system. We will present more detailed analysis of the individual events in future papers.

3. Data Analysis

LWA1 data are recorded as raw voltage streams without channelization. These data were processed first through the LWA Software Library tools [Dowell et al., 2012] using custom built Python scripts. Data were read from the LWA1 binary data format and processed through a Fourier transform spectrometer to obtain frequency-time spectrograms of the observation. Data are recorded in X and Y polarizations but are converted to the desired polarization basis of [X,Y], [R,L], or Stokes [I,Q,U,V] prior to constructing the spectrogram of the data. Frequency and time channelization are flexible and the standard configuration used for the Jovian observations allows for time bins as fine as 0.21 ms with associated frequency channelization as fine as 5 kHz.

All bursts were initially run averaging the full observing session data to a 2 second time interval with a spectral resolution of 10 kHz to provide a coarse time sampling of the entire burst structure. The goal of this process was to obtain an overview of the burst in Stokes I and V to examine the full burst structure and identify interesting regions for study. We present full-burst spectrograms of several events in Section 4. Once regions of Jupiter bursts were identified in the spectrum at 2 s resolution, higher time resolution power spectra were formed with resolutions of up to 0.25 ms. Details of the fine structure of the bursts are presented in Section 5.

Due to the wide instantaneous observing bandwidth of the LWA1, the instrument response will change across the observing bandwidth. Using our off-beams as well as the non-bursting sections of the Jovian beam we examined the shape and stability of the bandpass. In Figure 1 we show the median bandpass for the R and L polarizations for both the upper and lower tunings of an Io-A/Io-C burst observed 01-Dec-2012. These plots were made without any excision of radio frequency interference (RFI) using non-bursting times

Table 2. Jovian Burst Details

Date	MJD	Tunings (MHz)	Io-type	Polz.[1]	Io phase range (°)	CML III range (°)
10-Mar-2012	055996	26	Io-C	LHC/RHC	238.6 - 249.8	302.0 - 349.0
11-Mar-2012	055997	26	Io-B/Io-D	RHC/LHC	82.2 - 105.8	93.6 - 194.6
24-Sep-2012	056194	20, 28	Io-B	RHC	71.4 - 92.6	119.8 - 210.4
01-Dec-2012	056262	20, 28	Io-A/Io-C	RHC/LHC	210.7 - 253.1	184.2 - 5.6
27-Dec-2012	056288	22, 30	Io-B/Io-D	RHC/LHC	89.9 - 106.8	77.4 - 150.0
06-Mar-2013	056357	28	Io-A/Io-C	LHC/RHC	227.0 - 253.3	249.0 - 0.0

[1] Handedness of polarization observed in burst where first polarization listed is the dominant polarization.

of the Jovian beam. We see a slight offset in the power of the R and L polarizations which is due to a known offset in the X and Y dipole responses [Dowell, 2011; Ellingson, 2010]. We have calibrated the offset between the R and L polarizations using both the Jovian beam as well as a simultaneous off-beam on Tau A for several of our Jovian observing sessions. We find that the L polarization is consistently higher than the R polarization. The percentage difference between the two beams shows variations with time but remains below 5% for observations presented herein. This is reasonable since the observations were taken at the same frequency and at similar azimuth and zenith angles.

All data presented in this paper have been converted to Stokes V following the convention where positive Stokes V is RHC. We note that we cannot correct the bandpass of the individual polarizations during the bursting periods thus the Stokes V results will have a negative bias (due to the different R and L bandpass amplitudes) of up to 5% in the spectrogram plots. This offset is minor and does not impact the handedness of any emission presented in this paper. Furthermore, the circular polarization of Jupiter DAM emission events is shown to have little variation over long durations [Dulk et al., 1994].

The LWA1 has not yet been characterized for polarization response thus observations at large zenith angles are expected to have significant polarization leakage across the Stokes parameters. Determining the polarized response of a dipole array is considerably more difficult than for a single dish telescope. The reasons for this are: (1) dipole arrays produce beams with higher side lobe levels, therefore a significant contribution to the beam power comes from beyond the primary beam; (2) the dipole array beam shape and sensitivity vary significantly across the sky. The first factor violates the usual assumption that the source polarization properties are constant in time (or change only as a function of parallactic angle), and the second factor violates the assumption that the instrumental polarization is constant in time.

We have minimized the impact of the lack of polarization calibration by observing Jovian bursts at high elevations near transit. To characterize the impact of this leakage on the measured polarization, we have compared the fractional circular polarization measured for Jovian bursts with measurements from the literature. Using Io-B and Io-C bursts we have measured the fractional circular polarization of the emission over zenith angles from $\sim 20^\circ$ to over 50° and compared those measurements to statistical measurements of fractional polarization of the same type of bursts observed with the NDA as presented in Dulk et al. [1994]. We find very good agreement between the LWA1 measured fractional polarization and the NDA statistical results up to zenith angles of 40°. At larger zenith angles we see an elevation dependent fractional polarization which is due to the lack of polarization calibration. A similar effect is seen observing Cygnus A over a variety of zenith angles where the fractional circular polarization shows a slow increase with increasing zenith angle beyond roughly 50° (J. Hartman, 2012, private communication). We would not expect that the lack of polarization calibration would change the handedness of the emission observed and, in fact, we find that the handedness of the emission observed in all bursts recorded with the LWA1 matches that expected from the literature. Due to the lack of polarization calibration, we do not measure polarization fraction within this paper and report mainly the handedness of the emission as well as source structure.

RFI is present in the data in both persistent form with known emitters spread throughout the spectrum as well as intermittent RFI events [Obenberger & Dowell, 2011]. Observations were preferentially scheduled at night when RFI levels are lower but many of the observations had to be taken at least partially during the daytime to target high probability events in the observing cycle. For the majority of the Jovian observations, we found that the RFI only impacted a small amount of the spectrum and thus we have not excised these regions. During quiescent RFI times we were easily able to study Jovian emission down to frequencies of 12 MHz or lower (see for example Figure 3).

4. Morphology and Polarization properties of Several Io-Related Decametric Bursts

LWA1 observations of Jupiter were targeted during times of Io-controlled emission. In this section we present analysis of bursts from all four of the Io-controlled emissions regions. In Table 2 we list event details of each burst discussed in this paper while the observing session details are given in Table 3. In Figure 2 we show a probability plot of the Io phase vs CML III with the positions of Jupiter marked for each of the bursts discussed in this paper.

4.1. Io-A/Io-C

We show in Figure 3 a Stokes V spectrogram of an Io-A/Io-C event from 01-Dec-2012. The full observation lasts

Table 3. Observing Session Details

Date	Start Time (UT)	Duration (hours)	Sunrise (MST)[1]	Sunset (MST)	Elevation (°)
10-Mar-2012[2]	23:00:41	1.3	06:27	18:15	66 - 54
11-Mar-2012[2]	23:03:01	2.8	06:26	18:16	65 - 35
24-Sep-2012[2]	11:00:00	2.5	06:00	18:04	74 - 63
01-Dec-2012	08:15:00	5.0	06:58	17:01	68 - 7
27-Dec-2012	06:30:00	2.0	07:15	17:09	66 - 42
06-Mar-2013[2]	22:45:00	3.1	06:32	18:11	64 - 68

[1] MST zone (Mountain Standard Time) is UT-7 hours.

[2] Observing session includes at least some daytime data.

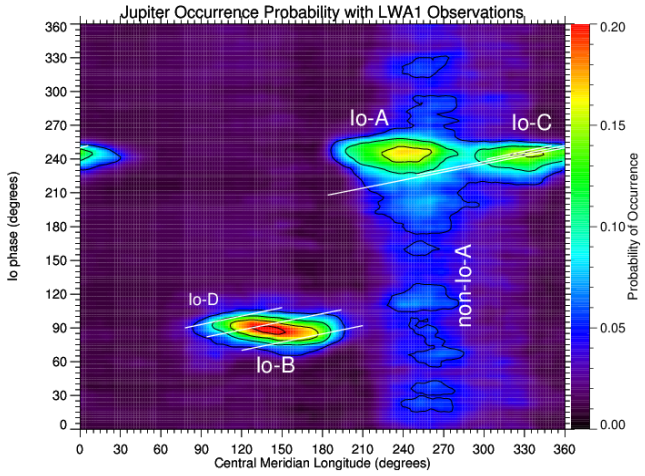

Figure 2. Occurrence probability plot showing the Io phase vs CML III. The probability of occurrence is shown in the color bar where the probability was determined from the work of Carr et al. [1983]. The white sloped lines show the regions of the Io phase vs CML III space probed by the Jovian bursts presented in this paper (see Table 2).

5 hours and we have combined the data from the two frequency tunings. The colorbar at the right shows intensity (labeled as power spectral density or PSD) with negative Stokes V (LHC) emission in blue and positive Stokes V (RHC) emission in red on a scale that is linear in power in arbitrary units. The ordinate axis shows observing frequency while the top abscissa is labeled in time since the start of the observation and the bottom abscissa is labeled in central meridian longitude system III (CML III).

The Io-A event (CML III 185° - 270°) shows classic vertex late arc structures, which are possibly caused by multiple Alfvén wave reflections between the Io plasma torus and the source regions [Queinnec & Zarka, 1998; Gurnett & Goertz, 1981]. We see additional (fainter) RHC emission between CML III = 270° to roughly 350° where it appears to drop below our observing frequency. This second RHC emission component appears distinct from the main Io-A emission; the overall intensity is weaker and the envelope reaches a higher frequency of ∼35 MHz. Boudjada et al. [1995] studied similar Io-C morphology using NDA data from 1986 to 1991 and identified one RHC component (called a great arc) and three LHC components (Type I, II, and III). They interpret their data as components of Io-C and suggest that both RHC and LHC emissions are coming from the same source in the same hemisphere. Recent modulation lane analysis (Section 5.1) also favors this interpretation; however, the different spectral structure and different frequency maxima of the RHC and LHC data are difficult to explain. We also note that bimodal polarizations emitted by the same source are not favored by theory [Melrose et al., 1984].

The LHC event begins at about CML III 230° and increases in frequency to reach a maximum frequency of ∼24.5 MHz before decreasing again in frequency to fall below our observing band around CML III=350°. We interpret this event as an Io-C burst but we note that it begins well before the generally accepted beginning value of CML III=280° for Io-C events [Carr et al., 1983]. Although the previously published source boundaries are based on long-term statistics and are frequency dependent, individual Io-C events beginning at values prior to CML III 280° have been shown before [e.g. Ray & Hess, 2008; Boischot et al., 1981]. The CML boundaries were not previous discussed, however, these new LWA1 observations suggest that the CML III range for the Io-C source needs refining. More precise source boundaries will be of value to theorists and modelers to better know the active CML regions and their associated magnetic field lines. Furthermore we hope the LWA1 data can help disentangle the Io-A from the Io-C source(s) and be used to determine the hemispheric source(s) for the Io-A and/or Io-C components.

The vertex late arc structures characteristic of Io-C events are clearly seen by the LWA1. In Figure 4 we show a higher resolution section of the LHC polarization in the lower frequency tuning for the portion of the burst from 10800 s onward. We can clearly see that the Io-C event splits into at

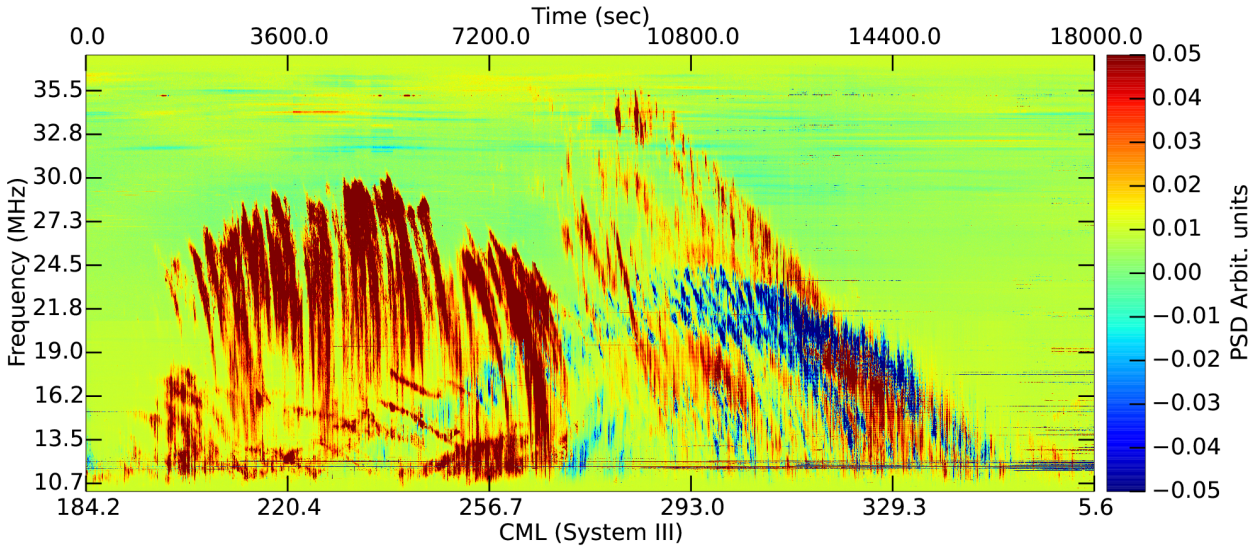

Figure 3. Io-A/Io-C burst recorded 01-Dec-2012 for a total duration of 5 hours. Both the upper and lower tunings have been merged to show the entire frequency range covered along the Y axis. The elapsed time since the start of the observation is shown in the upper axis while the CML III range in shown on the lower axis. The color scale is the power spectral density in arbitrary units shown in the right color bar. On this scale right hand circular emission is in red while left hand circular is in blue.

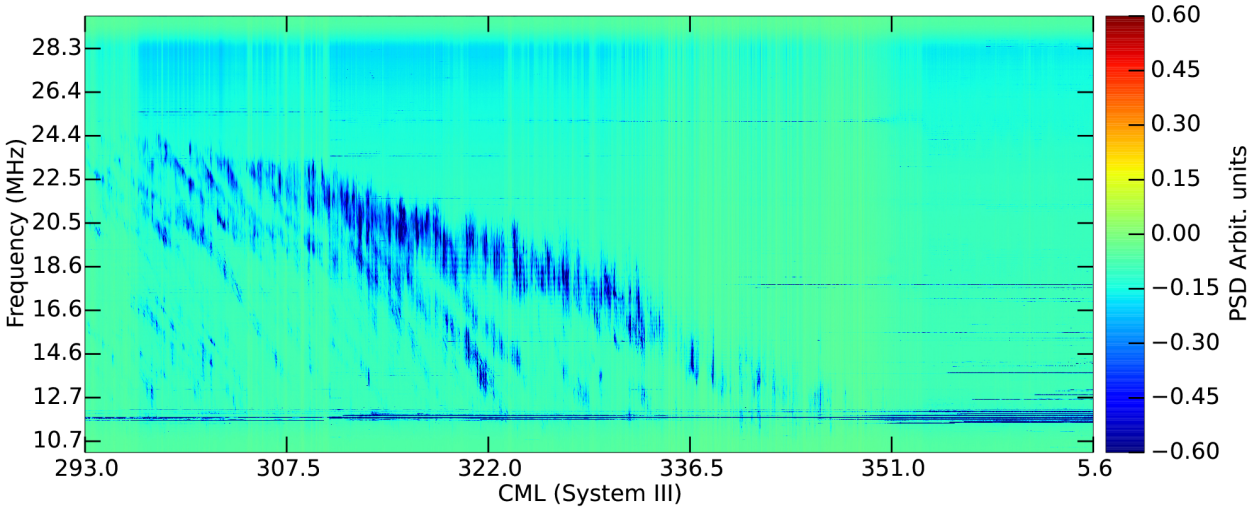

Figure 4. Segment of the Io-C burst seen in Figure 3 shown in higher resolution from CML III=293.0° to the end of the burst. The LHC polarization clearly splits into at least two different structures.

least two different structures near the end of the event. The very subtle, nearly horizontal amplitude modulations seen near 19 MHz in the burst emission are ionospheric Faraday lanes induced in the highly elliptically polarized emission as it passes through the Earth's ionosphere (see Figure 13 for more obvious Faraday lanes).

We have observed two other Io-C events with the LWA1 and find remarkable similarity in the events. In Figure 5 we show the upper frequency tuning (centered on 26 MHz) for an Io-C event from 10-Mar-2012. RHC emission is seen from the observation start at CML III = 302° until CML III = 323°, where the emission drops below an observing frequency of 17 MHz. The LHC emission is seen from the observation start until it falls below our band at ∼ CML III = 342°. Similar to the burst described above, we interpret the RHC emission as a 'Great arc' and the LHC emission as Io-C, most likely coming from the southern hemisphere. The Io-C emission reaches a maximum frequency of roughly 25 MHz and shows the same vertex late arc structures as the previous burst.

The third Io-C event we present, Figure 6, was observed on 06-Mar-2013 for a total of 3.1 hours. The early portion of the observation shows the Io-A emission in RHC ending around CML III = 268° while the LHC emission of the Io-C event starts around CML III = 277° and runs past the end of our observing window. As with the other two events discussed above, the Io-C emission shows the vertex late structure typical of these events. We measure a peak frequency of just above 24.6 MHz for the LHC Io-C emission. Similar to the other two events, we also see the great arc RHC emission co-incident with the Io-C event between CML III of roughly 275° and 318° before it drops below our upper tuning frequency. Although the lower tuning is significantly impacted by RFI, we are able to continue tracing all RHC and LHC emission to frequencies near 12 MHz.

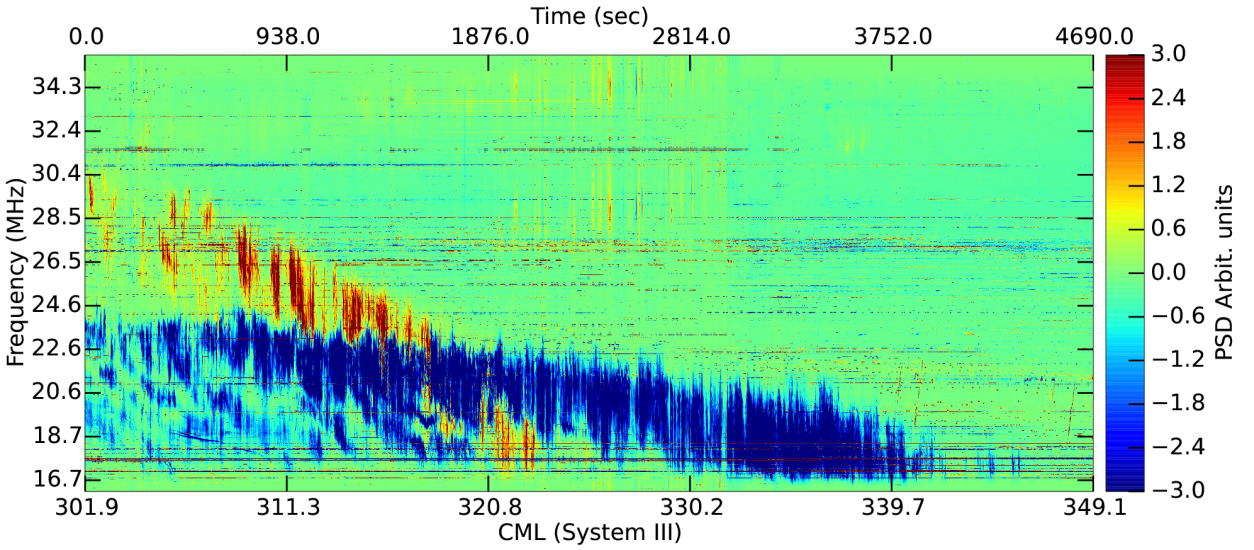

Figure 5. Upper tuning (centered on 26 MHz) Stokes V spectrogram of an Io-C burst recorded 10-Mar-2012 for a total duration of 1.3 hours.

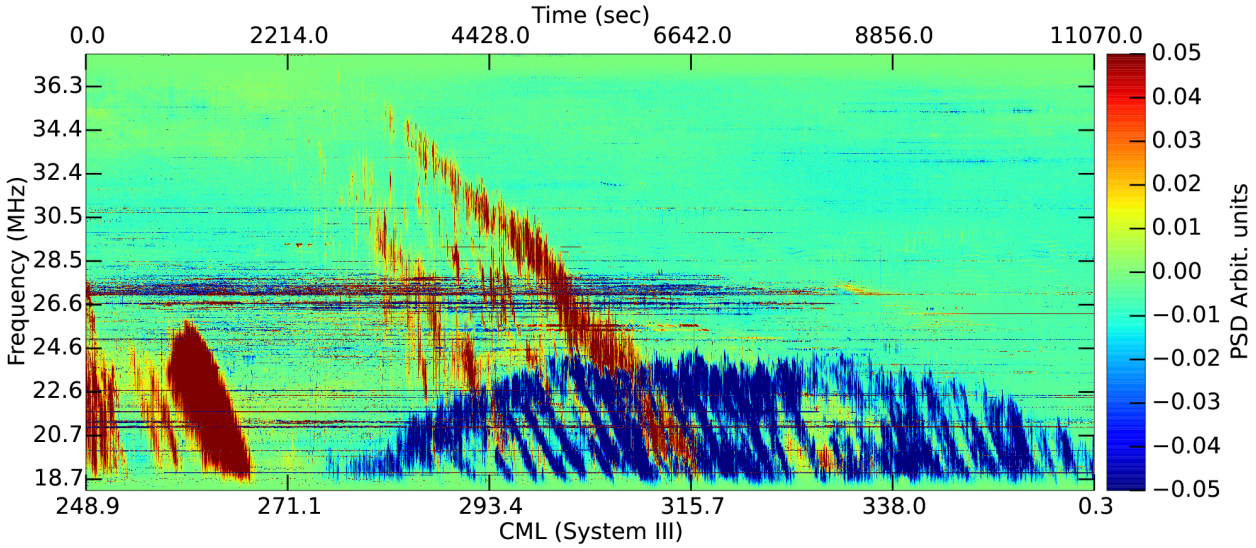

Figure 6. Io-A/Io-C burst recorded 06-Mar-2013 for a total duration of 3.1 hours. Only the upper tuning (centered at 28 MHz) is shown as the observations were taken during the daytime and the lower tuning was severely impacted by interference. During the early parts of the burst the RHC Io-A emission is seen and later the LHC Io-C emission is visible. Between CML III $\sim 280°$ to $316°$ we see RHC emission similar to that in Figure 3.

Comparing the three events in Figures 3 to 6 we see that the overall picture is one of the Io-A event ending before CML III = 270° followed by a RHC event which proceeds from higher frequencies (35 MHz) around CML III = 270° to lower frequencies reaching CML III up to 350° before falling below our lowest frequency observing window. More surprisingly, the LHC Io-C events appear to start at CML III as early as 230° at low frequencies (11 MHz), peaking at roughly 25 MHz near CML III of 300° to 315° before falling again to frequencies as low as 11 MHz near CML III of 345°. The most recent event reported here (06-Mar-2013) appears to have the Io-C emission shifted in CML III by at least 20° compared to the event observed one year earlier. The typical CML III range quoted for Io-C events is 280° - 60° [Carr et al., 1983].

Observations of Io-A/Io-C storms with the NDA are suggestive of an early start to the Io-C[3], but there has not been any discussion or publications regarding the boundaries of the Io-C source. In panel b of Figure 1 in Boudjada & Genova [1991] we see the RHC and LHC emission from an event on 15-Oct 1987 that shows structure remarkably similar to the events presented herein in Figures 3 to 6. Boudjada & Genova [1991] note the occurrence of the LHC Io-C emission in the same CML III range as the RHC but do not trace the early start due to significant RFI present in the data below 20 MHz.

Polarization studies of Jovian decametric emission using Voyager planetary radio astronomy (PRA) data by Alexander et al. [1981] reported a change in the handedness of circular polarization of continuous DAM emission below 15 MHz. Ortega-Molina & Daigne [1984] showed that these anomalies and sign reversals in the polarization of the PRA below 15 MHz can be explained by the antenna response when the dipole length is close to the observing frequency. Using a model for the polarization response for the PRA, Ortega-Molina & Lecacheux [1991] were able to analyze the polarization properties of the hectometric emission and separate the contributions of two main sources of emission. They found these two sources had opposite handedness and independently changing intensities. Due to the complexities of the higher frequency PRA band, they were not able to map the polarization details of the DAM. At these higher frequencies from Voyager only total intensity analyses of Jupiter's DAM were made and thus it would have been very difficult to detect the early start of the Io-C emission we observe with the LWA1.

4.2. Io-B

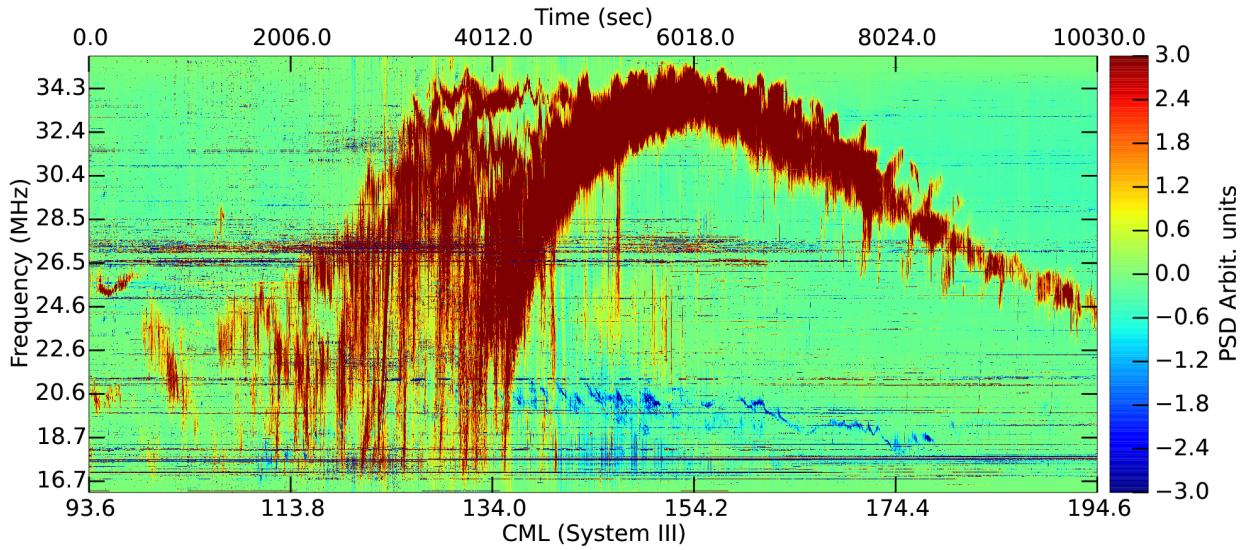

Figure 7. Upper tuning (26 MHz) for the Io-B burst recorded on 11-Mar-2012. The RHC emission from the Io-B event peaks at frequencies near the upper end of our observing window ($\sim$ 35 MHz) and is seen to cover the full observing time. We also see faint, narrow-band LHC emission peaking near 21 MHz which we interpret as Io-D emission.

Io-B events are generally considered as originating in the northern hemisphere and are thought to represent the leading edge of the northern emission cone. In Figure 7 we show the upper tuning (centered at 26 MHz) of a classic Io-B observation from 11-Mar-2012. Early in the event we see emission drifting upward in frequency and peaking about 35 MHz followed by a more narrow-band tail that drifts downward in frequency. The Io-B source shows vertex early arc structure that have been well studied and modeled [Hess et al., 2008; Queinnec & Zarka, 1998; Wilkinson, 1989; Leblanc, 1981; Goldstein & Thieman, 1981]. As is common in Io-B events, S-bursts are seen in the early part of the event. We also see a faint, and more narrow-band LHC emission ranging from CML III values of about 130° to 180°. This emission peaks about 21 MHz and is most likely southern hemisphere Io-D emission. We discuss S-bursts in Section 5.3.1 and the Io-D emission in Section 4.3.

A very different Io-B event showing a series of narrow-banded emission regions is shown in Figure 8. This observation covers a total of 2.5 hours. This entire event consists of narrow-band emission bands. Analysis of the high temporal resolution spectrograms of this burst show a number of fine structure details such as S bursts and Tilted V events. These latter events are seen as regions within narrow-band events that are bounded

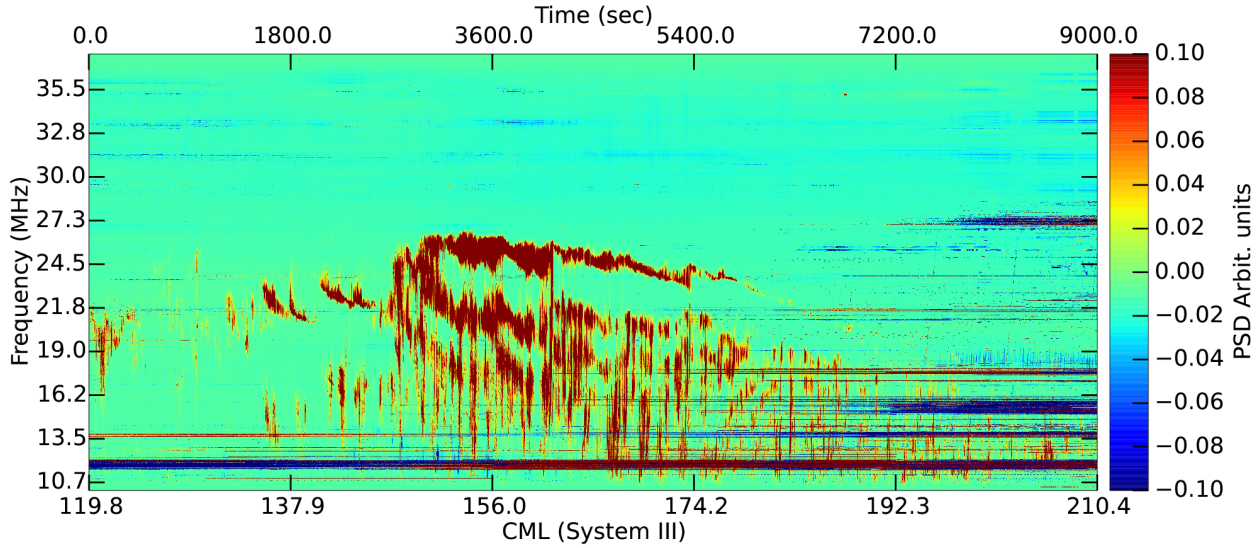

Figure 8. Narrow band Io-B burst recorded 24-Sept-2012. The burst is comprised of narrow bands of S-bursts and N-events and is host to a variety of features including the Tilted-V events described in [Riihimaa, 1990].

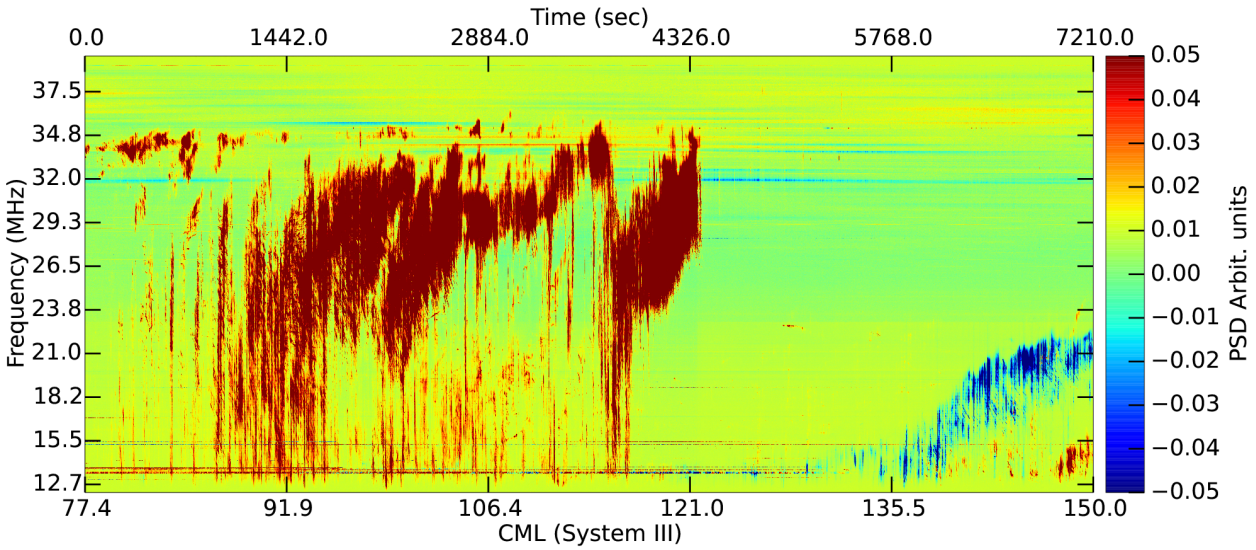

Figure 9. Io-B event from 27-Dec-2012 which shows vertical arc structures and a maximum frequency of 35 MHz. A sharp cutoff of the emission occurs at (CML III 121°, Io Phase 100°), just as the source exits the Io-B region (see Figure 2). At later times, Io-D emission is clearly evident beginning about (CML III 130°) and reaches a peak frequency of 22.5 MHz.

by two S bursts [Riihimaa, 1990] and are discussed further in Section 5.3.1.

The final Io-B/Io-D event we present is shown in Figure 9. This event is peculiar because the Io-B emission cuts off sharply at 07:43 UT (CML III 121°, Io Phase 100°), presumably just as the source cone rotates past the Earth. Because the LWA1 off-beam data (not shown here) show good continuity over this interval, we believe that this sharp cutoff is real and displays the narrow beaming nature of the DAM emission cones. Figure 2 shows that this event was a high pass through the Io-B probability region on the Io phase-CML III plane. Soon after the Io-B cone moves out of our line of sight an Io-D event begins. This event is seen as the LHC emission. Unfortunately this observation ended at 09:40 UT (CML III 150°, Io Phase 107°) just as Io-D appeared to be reaching its peak frequency. The maximum frequency observed before the end of the observations was 22.5 MHz. This Io-D event is also particularly interesting due to the detection of S-bursts within it (see Section 5.3.2).

4.3. Io-D

The leading edge of the southern emission cone is thought to be associated with Io-D events. These sources are more elusive due to the lower emission intensity, lower emission frequency and the overlap of the source emission region with the same general CML III and Io Phase (Φ_{Io}) range as the stronger Io-B radiation. The CML III and Io phase ranges for the Io-D source are CML III = 0° to 200° and Φ_{Io} = 80° to 130° [Carr et al., 1983]. Queinnec & Zarka [1998] found that the Io-D reaches down to frequencies of 3 MHz and that it appears as an isolated arc. Their model argues for the Io-D source in the southern hemisphere along a single Io flux tube. We note that we did not specifically target Io-D events during our initial observing program but several events were detected within the targeted Io-B event observations. Based on these detections, we have initiated a follow-up observing program which specifically targets the Io-D sources for detailed structure analysis and those results will be presented in a future paper.

In Figure 7 we see evidence of weak, narrow-band LHC polarization extending over CML III = 134° to 185° and Φ_{Io} = 93° to 104°. The emission is slowly drifting in time with the peak frequency moving from a maximum near 21 MHz to around 18 MHz. The emission characteristics of this Io-D event are consistent with results from both NDA and Voyager data [see Leblanc, 1981; Hess et al., 2008]. Structures identified in higher time-resolution images of this LHC emission are discussed in Section 5.3.2.

The second Io-D event we present can be seen beginning near the end of the 27-Dec-2012 event shown in Figure 9. Shortly after the Io-B emission cone passes out of our line-of-sight, the LHC Io-D emission begins. The emission is initially at very low frequencies ($\sim$ 13 MHz) near CML III 121°. The emission frequency increases until the end of our observations at which point the peak frequency is near 22 MHz. Due to the remarkably clean radio frequency interference spectrum at these low frequencies we are able to see evidence of both Riihimaa modulation lanes as well as nearly horizontal, closely spaced Faraday lanes that are clearly seen below 21 MHz across both the Io-B and Io-D emission regions. We show these Faraday fringes in Figure 13 and discuss this further in Section 5.2. High time-resolution study of this Io-D burst shows clear S-burst structure within the event. In Section 5.3.2 we

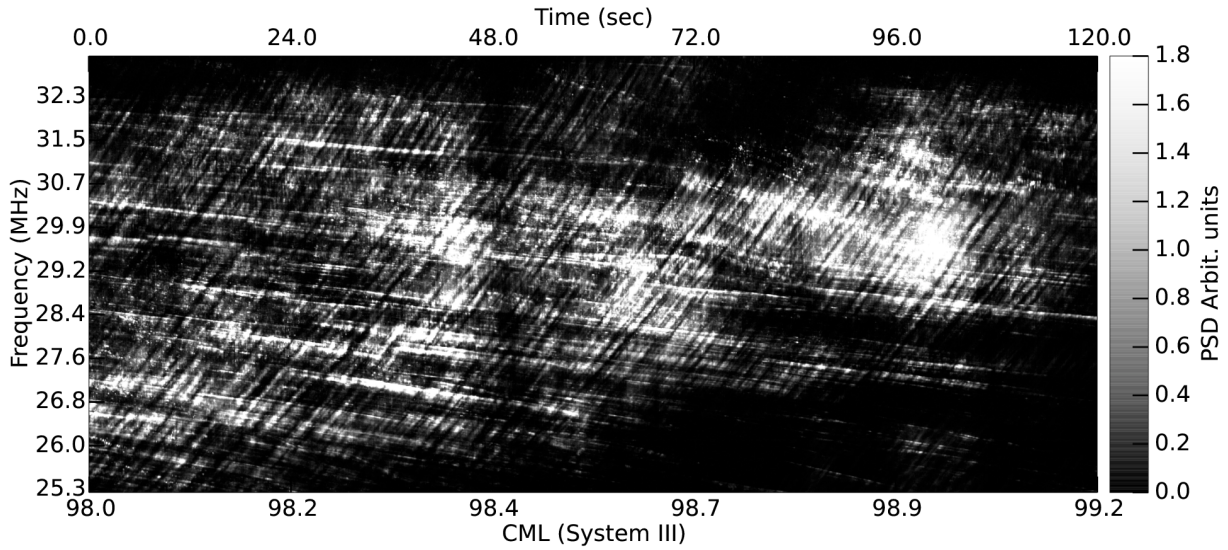

Figure 10. Positive slope modulation lanes seen in a portion of the Io-B burst of 27-Dec-2012 which is shown in Figure 9. The image is made with a temporal resolution of 10 ms and spectral resolution of 10 kHz.

discuss the rare Io-D fine structure and characterize the drift rate of these S-bursts.

5. Modulation Lanes and Fine Structure

There are many examples of fine structures clearly seen in the LWA1 data. Most of these structures have been seen by other ground-based and spacecraft observers [Litvinenko, 2009; Zarka, 1998; Carr et al., 1983] in one or more Io-controlled events. Examples include frequency envelopes for different sources, nested arc features, narrow band events, modulation lanes, Faraday lanes, and simple and complex S-bursts. We will highlight many of the excellent LWA1 observations and address these features in the sections below.

5.1. Modulation Lanes

Jovian emission undergoes a variety of propagation effects as it passes from the emission cone near the planet through the magnetoionic plasma in the Io torus, the interplanetary medium and the Earth's ionosphere. Riihimaa [1968] identified a set of amplitude modulation lanes that cut across the L-bursts and S-bursts and which could have either positive or negative slopes. These modulation lanes are characterized by a strong periodicity in time, with periods ranging from about 1 to 5 sec and an average of about 2 sec.

In Figure 10, we show a small 120 second portion of the Io-B event shown in Figure 9 where positive slope modulation lanes are clearly visible. This image has a temporal resolution of 10 ms and spectral resolution of 10 kHz. The modulation lanes show regular spacing crossing the Io-B emission. Slope measurements of the lines in the frequency range of 21-23 MHz in early parts of this 27-Dec-2012 event show slopes consistent with measurements from Riihimaa [1968].

High temporal resolution spectrograms of the 10-Mar-2012 event show modulation lanes visible through the RHC and LHC emission of this event (Figure 12). Analysis of these lanes shows that they are continuous across the two different polarization hands [Imai, 2013]. We defer a detailed analysis of this modulation lane structure to a future paper but do note that the detection of these modulation lanes may have very important implications for our understanding of the emission mechanism at Jupiter. If both the RHC and LHC emission regions are shown to be crossed by continuous modulation lanes then, according to the widely accepted Imai et al. [1992] model, this would mean that the two polarization hands must be coming from sources in the *same* hemisphere. This would then suggest that the emission detected would be both the L-O and R-X modes of the CMI. One concern is that theoretical studies of the CMI emission mechanism of Earth's auroral kilometric radiation (AKR), which is analogous to Jovian DAM emission, predict that the R-X mode growth rates up to two orders of magnitude larger than the L-O mode [Melrose et al., 1984]. Observational studies of AKR support these predictions [Hanasz et al., 2003]. Our data show roughly similar powers for both hands of polarization which may imply that other processes are necessary to explain the L-O emission, like refractions, reflections, or mode conversions. Alternately, if the emissions are coming from opposite hemispheres, the propagation paths of each source emission through an interference screen that is comprised of field-aligned columns of enhanced plasma density from the Io torus would need to be remarkably similar to form the continuous modulation lanes across both polarizations [see Imai et al., 1997].

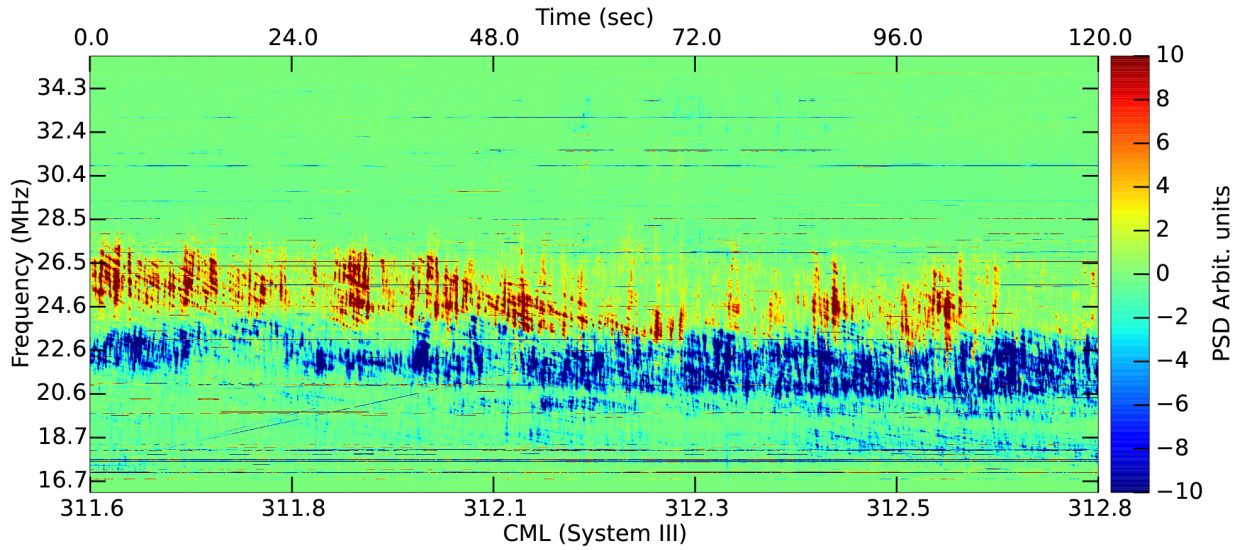

Figure 12. Zoom in of the Io-A/Io-C burst recorded on 10-Mar-2012 showing 120 seconds of data starting at 23:16:41 UT. Modulations lanes are visible as negative drifting features (decreasing frequency with time) running through the LHC and RHC emission. The two LHC features running from low to higher frequencies seen from the beginning of the observation to the middle are ionospheric sounders. Color bar as in Figure 3.

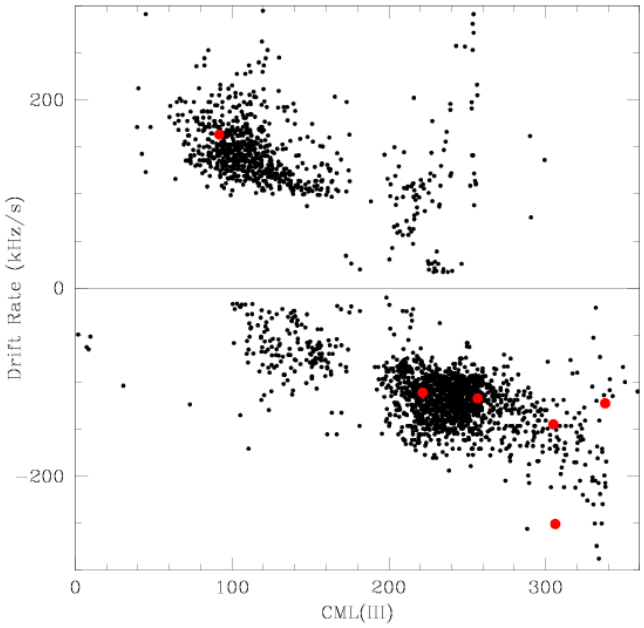

Figure 11. Modulation lane slope vs CML III plotted for data from Riihimaa [1968] in black with measurements from the LWA1 bursts shown as red points. Each LWA1 slope measurement is the mean of 6 independent slope measurements taken in nearly adjacent lanes around the CML III value. Each point is measured for lanes in a single burst but multiple bursts were used for the range of measurements shown.

We have measured the slope of the modulations lanes for the above LWA1 events. We show in Figure 11 the measured slopes of several of the LWA1-detected modulation lanes included on the modulation lane plot of Riihimaa [1968]. Each LWA1 slope is the mean of independent slope measurements for 5 consecutive modulation lanes around the plotted CML III. The figure shows the modulation lane slopes we measure are consistent with earlier papers although we note that we do detect modulation lanes in Io-C regions of the plot that are currently sparsely populated. We defer a detailed modulation lane slope analysis with many more measurements to a future paper.

5.2. Faraday Fringes

Highly elliptically polarized emission passing through dense plasma media, such as Jupiter's Io plasma torus plus magnetosphere and the Earth's ionosphere, will undergo Faraday rotation due to the bi-refringent nature of the magnetized and ionized plasma.

Each magneto-ionic medium between the source and observer will introduce a rotation measure (RM) in the polarized Jovian emission where Rohlfs & Wilson [2004] show the Faraday rotation measure along some path ℓ is defined as:

$$RM = \frac{e^3}{2\pi m_e^2 c^4} \int_0^\ell n_e(s) B_\parallel(s)\, ds \quad \text{radians/m}^2 \quad (1)$$

where e is the electron charge, m_e is the mass of the electron, c is the speed of light, n_e is the electron density at each point s along the path, and $B_\parallel$ is line of sight component of the magnetic field at point s.

There are at least four distinct contributions to the observed Faraday rotation of Jovian decametric emission. These are (1) the Jovian magnetosphere, (2) the Io plasma torus, (3) the interplanetary medium, and (4) the Earth's ionosphere. Each of these components

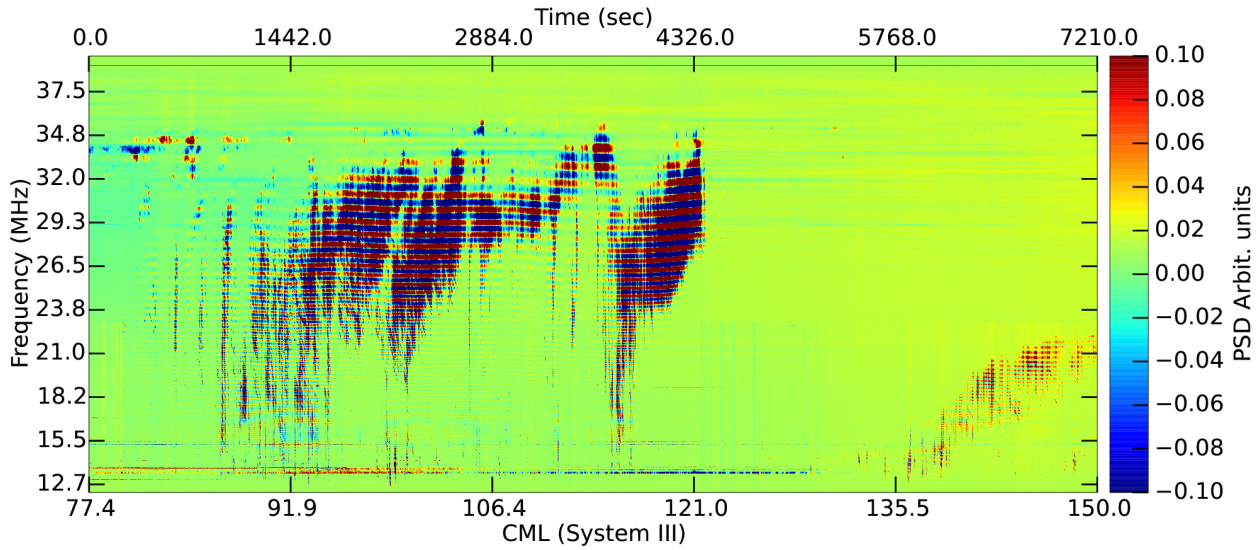

Figure 13. Plot of 27-Dec-2012 burst showing Faraday fringes in a linear polarization difference spectrogram. The nearly horizontal Faraday fringe bands are seen across the entire Io-B and Io-D emission regions. The fringe separation decreases as the frequency decreases due to the λ^2 nature of Faraday rotation.

will make a time-variable contribution to the observed Faraday rotation. Taking into account the propagation effects from these media, Dulk et al. [1992] used Io-B events observed from the NDA to determine that at least some of the Faraday rotation comes from the Io plasma torus. The fraction of Faraday rotation from each of the components above is unclear from work in the literature and is discussed in some detail in Litvinenko [2009]. The majority of the RM signal likely comes from the Earth's ionosphere which has typical electron density of $n_e = 5 \times 10^5$ cm^{-3}, field strength of $B_{\|} = 0.3$ G, and a path length of 500 km. This results in a contribution of roughly RM$_{\oplus} \sim 2$ rad/m^2.

Linearly polarized feeds, such as used at LWA1, will detect the emission with a time-variable visibility in each of the two orthogonal polarizations. We have investigated several of the bursts using the orthogonal linear polarizations from the LWA1 and see clear evidence of Faraday fringes. We show in Figure 13 a linear polarization difference spectrogram of a portion of the 27-Dec-2012 Io-B/Io-D event with clear nearly horizontal Faraday fringes. Similar Faraday fringes have been seen for the Io-B event on 11-Mar-2012. We have used the locations of the nulls in the latter event to determine the rotation measure of RM=2.2 rad m^{-2} which is similar to the expected contribution from the Earth's ionosphere.

5.3. Fine Structure

In this section we discuss some of the fine structure seen in the LWA1 observations of the Jovian bursts. Short bursts of emission, known as S-bursts, are described in detail in [Zarka et al., 1996; Carr et al., 1983]. These sources consist of a series of very short pulses of emission that range in length from 1 ms to several hundred ms. The instantaneous emission is very narrow in frequency and typical drift rates are between -5 and -30 MHz/s [Zarka et al., 1996]. Drift rates have been measured for S-burst seen in Io-B and Io-C events, and more rarely in Io-A events [Hess et al., 2009; Flagg et al., 1991]. Assuming that the emission occurs near the local electron cyclotron frequency, the negative slope is interpreted as resulting from motion of the packet of radiating electrons away from the Jovian surface toward lower magnetic field strengths. Carr & Reyes [1999] show the fine structure within an S-burst and the coherence of the oscillations inside the microstructure while wavelet analysis of these bursts shows modulations on scales of 6-15 μs [Litvinenko et al., 2004].

N-events are described in Riihimaa [1985]. These events are relatively rare and consist of narrow frequency bands with trains of emission that can drift up or down with time. The N-events are often either composed of short S-bursts of multiple 'split' bands of emission. Typical bandwidths are 200 - 600 kHz with durations of a few seconds to tens of minutes. These events are also seen to drift slowly in frequency with time in some cases. Riihimaa [1968] studied the occurrence of the N-events and found they are often seen over a wide range of CML III.

5.3.1. Io-B Fine Structure

We have investigated the fine structure of the 11-March-2012 Io-B event (Figure 7) at high temporal resolution. Figure 14 shows a short ~ 1.8 s long portion of the burst with 0.25 ms temporal resolution and 10 kHz spectral resolution for a 9.2 MHz wide frequency window centered around 21.8 MHz. We see that the portion of the spectrum between 21 and 25 MHz is largely dominated by S-bursts while below 21 MHz there is a mix of S-bursts and N-events. We have measured the slopes

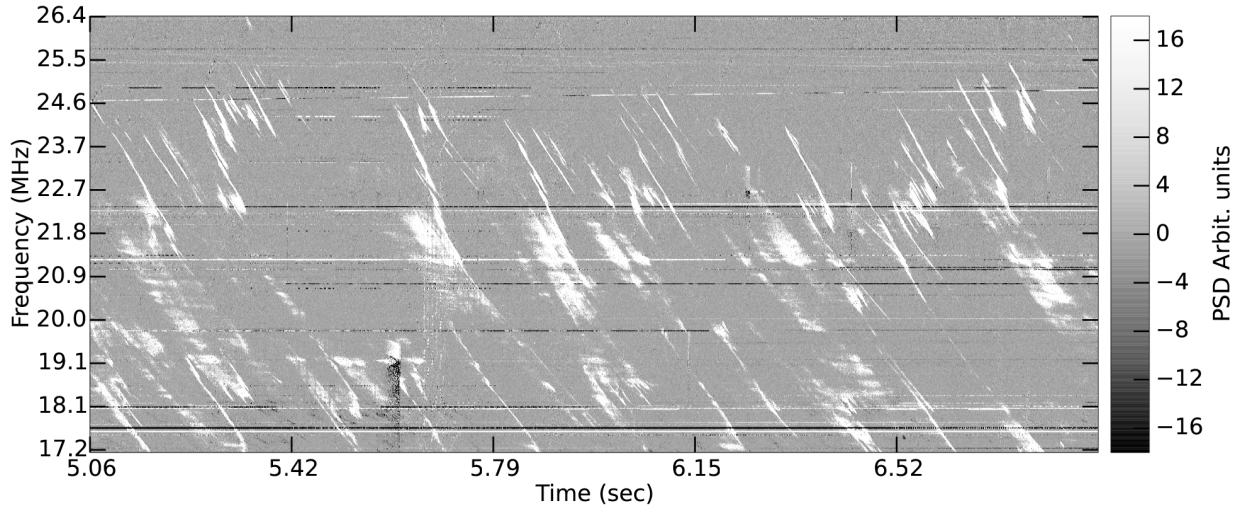

Figure 14. Multiple S-bursts plotted at 0.25 ms and 10 kHz resolution over 1.825 seconds of the 11-March-2012 Io-B event. The S- and N-events show apparent destructive interaction of the two bursts.

of the S-bursts in several regions of the Io-B event and find values of around -15 MHz/s, consistent with typical values for Io-B events reported in the literature [see Figure 3 in Zarka et al., 1996].

More complex S-burst interactions with N-events are seen below 23 MHz in Figure 14 where there appears to be multiple instances of N-events terminating at the time when an S-burst passes through the same frequency as the N-event. In Figure 15 we isolate details of one such interaction over a total time of 0.21 s. This figure shows the full details of one S-burst that starts near 25.6 MHz and drifts at a rate of -17.9 MHz/s to roughly 23.7 MHz where it encounters and apparently quenches an N-event which began $\sim$ 15 ms before the S-burst encounter. Multiple S-bursts appear to be generated after the termination of the N-event starting at frequencies of 23.2 MHz and with slopes of -16.3 MHz/s. Analysis of high temporal resolution data on this event appears to show that there are several regions where the S-bursts and short N-events are apparently interacting. This would suggest that the source regions for each type of event are cospatial.

Previous observations have been made that show interactions between N-events and S-bursts, referred to as S-N burst events [Oya et al., 2002; Riihimaa, 1985; Riihimaa & Carr, 1981]. The S-N burst events typically occur between 20-24 MHz and show an inverted tilted-V shape in the spectrum that connects the S-burst with the N event. Figure 16 shows a 4.3-second portion of one of the narrow bands of emission during the 24-Sept-2012 narrow-band Io-B event (see Figure 8). The spec-

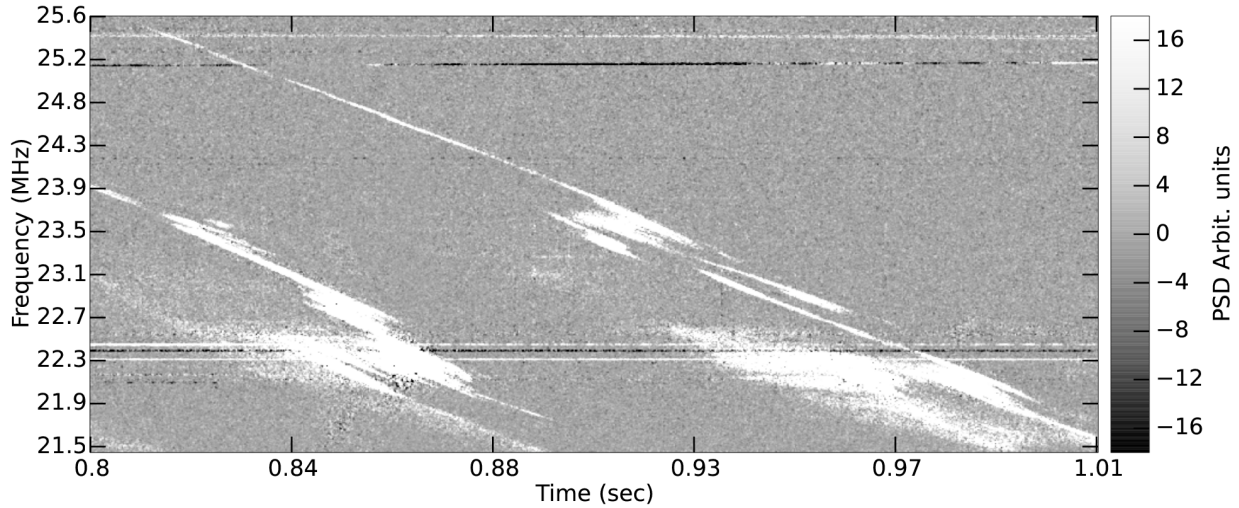

Figure 15. Zoom in on a single S-burst at 0.25 ms temporal resolution and 10 kHz spectral resolution over a total of 0.21 s during the 11-March-2012 Io-B event.

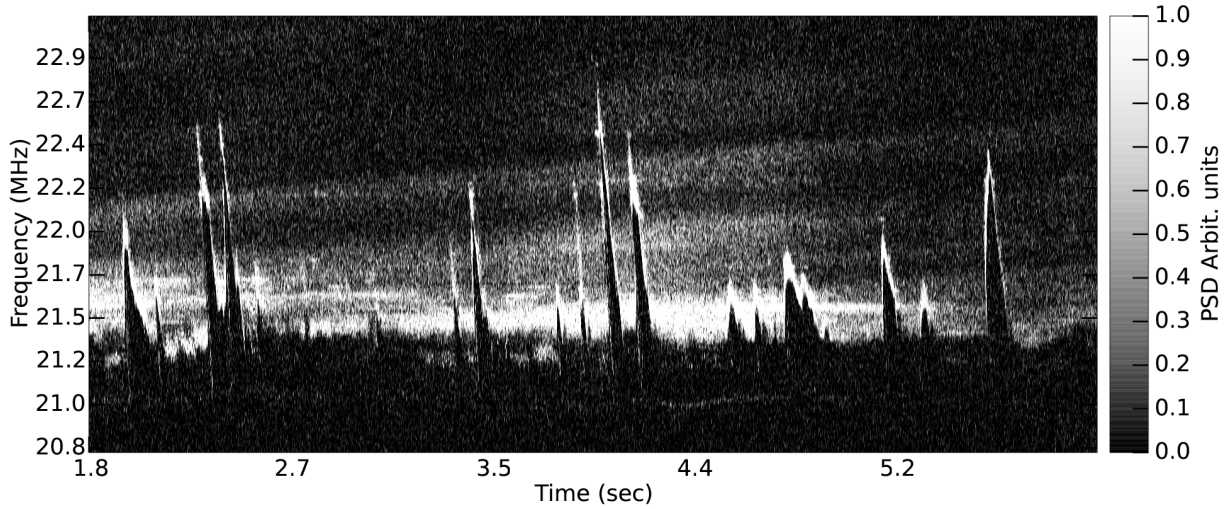

Figure 16. This spectrogram, shown in black-and-white for clarity, shows one of the narrow bands of Io-B emission during the 24-Sept-2012 event seen in Figure 8. More than a dozen inverted tilted-V shaped narrow band emissions are seen in this 4.3 second spectrogram. The emissions have a baseline frequency of about 21.3 MHz and are seen to fluctuate rapidly to frequencies as high as 22.7 MHz and back over 0.1 seconds. Also seen are the shadow event regions of near zero emission beneath the tilted-V shapes.

trogram in Figure 16 has a bandwidth of 2.3 MHz centered on 22 MHz and clearly shows many inverted-V shapes as narrow band emissions changing rapidly in frequency and in time. Also seen are the shadow event regions beneath the tilted-V shapes. The origin of these events and interactions are not clearly understood, but are thought to be bunched electrons accelerated by electric fields upward along the Io flux tube [cf. Oya et al., 2002, and references therein]. Thus these S-N burst events are believed to be generated in the same region in Jupiter's magnetosphere; our observations of S- and N-events shown in Figures 14 and 15 are consistent with this interpretation. More high resolution observations of the Io-B source using the LWA instrument may provide some additional clues as to the nature and origin of these peculiar events.

5.3.2. Rare S-Bursts in an Io-D event

Very little information is available in the literature regarding the Io-D events. In general, the Io-D emission seems to be characterized by relatively narrow emission

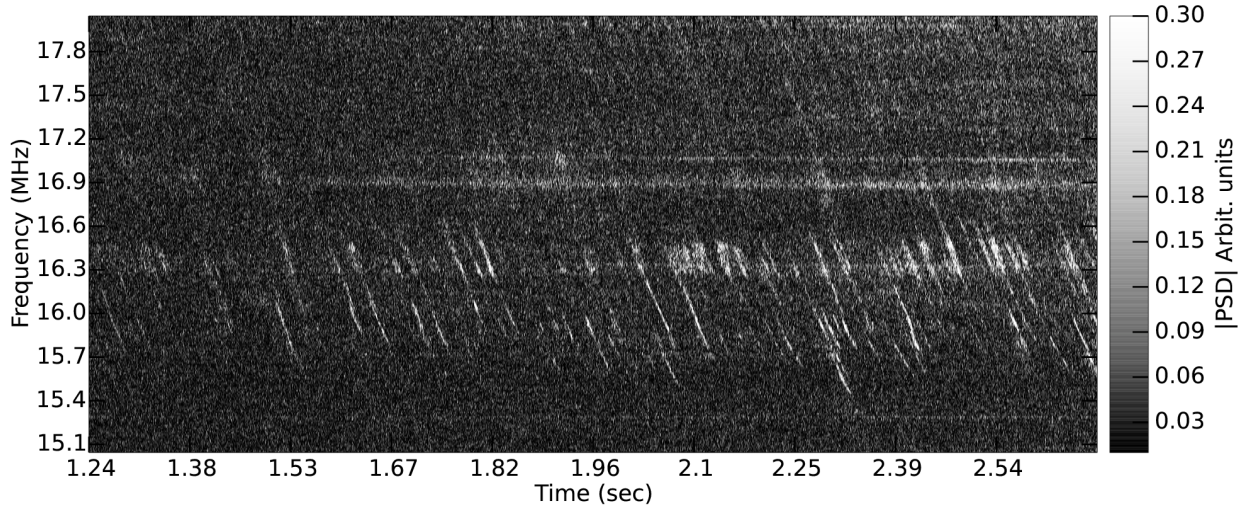

Figure 17. S-bursts for the Io-D event on 27-Dec-2012 (see Figure 9) plotted at 0.25 ms temporal resolution and 10 kHz spectral resolution. The bursts are LHC but are shown in the figure as an absolute value in greyscale to enhance the visibility of the bursts. Times are shown relative to 6236 seconds into the burst with a total time of 1.44 seconds displayed.

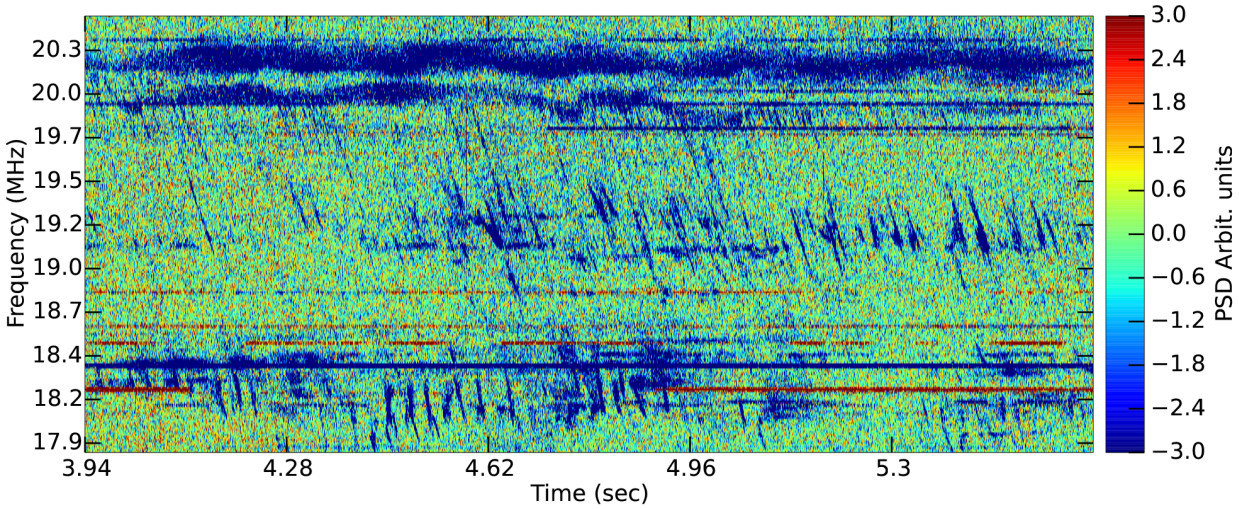

Figure 18. S-bursts for the Io-D event on 11-March-2012 (see Figure 7) plotted at 0.25 ms temporal resolution and 10 kHz spectral resolution. Narrow-band emission as well as S-bursts are seen within the LHC Io-D emission.

seen over a wide range of CML III and confined to frequencies below $\sim$ 18 MHz [Carr et al., 1983].

We have undertaken high temporal resolution studies of the Io-D emission from the 27-Dec-2012 event and we see clear S-bursts during this LHC emission event. A short portion of the spectrum ($\sim$ 1.44 s) is shown in Figure 17 where we show the region of the spectrum from $\sim$ 15 MHz to 18 MHz. We measure drift rates of the Io-D S-bursts of -11 to -15 MHz/s at frequencies of 15 to 16 MHz which are consistent with drift rates from other Io sources. There are few discussions in the literature regarding S-burst detections during known Io-D events, and only one definitive event could be found in the literature [see Litvinenko et al., 2010]. Because both Io-B and Io-D have significant overlap in CML, it is difficult to distinguish the Io-related source of the S-bursts. There is some possible evidence showing Io-D related S-bursts in the Voyager PRA data (see Alexander & Desch [1984]) and Cassini radio and plasma wave science (RPWS) data (see Lecacheux et al. [2001]).

In Figure 18 we show the details of the LHC Io-D emission from the 11-March-2012 event with 0.25 ms temporal resolution and 10 kHz spectral resolution. The figure shows a window of 1.7 s and a frequency window of 2.6 MHz centered around 19.1 MHz. The emission is seen to consist of several narrow bands of emission at frequencies near 20 MHz as well as S-bursts at frequencies between 18 and 20 MHz. We note that the horizontal structures seen in the figure are RFI. Analysis of additional sections of the Io-D emission show structures such as tilted-V events and other narrow-band structures.

More observations are currently being conducted in an effort to further characterize the fine structure of the Io-D events which can be useful in understanding the electron acceleration method and the source generation mechanism.

6. Summary

The Long Wavelength Array (LWA1) instrument is shown to be an excellent instrument for studies of Jupiter decametric radio emission (DAM). The large bandwidth, fine spectral and temporal resolution, and full Stokes capabilities of the LWA1 instrument allow for a comprehensive analysis of Jupiter's broad and fine DAM structures. The location and low RFI environment are suitable to measure Jupiter's emissions down to about 11 MHz, well below most other Earth-based radio telescopes. This overview paper of targeted Io-related Jovian DAM emissions not only highlights the capabilities of the LWA1 instrument, but also provides some new data and insight into the nature of Jupiter's decametric emissions. The Jupiter observations from Dec-2011 to Mar-2013 highlighted in this paper show good Io-A, Io-B, Io-C, and Io-D structures, and the broad and fine detail in these data are further enhanced by the excellent polarization capabilities of the LWA1 instrument. Data reduction and analysis show some characteristic Io-related spectral signatures but also show some fine structures and details not seen before. A summary of the findings follows.

The Io-A observations show characteristic vertex-late arc structures as well as some narrow band emission events at frequencies below 19 MHz (see Figure 3). The remarkable observations are the Io-C emissions that occur simultaneously with the Io-A emissions. The onset of the LHC Io-C emissions at 11 MHz was measured to be CML III 230°; this has not been clearly measured before and allows the extent of the Io-C source to be sig-

nificantly expanded. The CML range of the Io-C source can tentatively be defined as CML III $230° - 60°$ [Carr et al., 1983, previous range was $280° - 60°$]. Further observations are warranted, but this can give clues to the nature and geometry of the southern hemisphere emission regions and be of value to new decameter emission models. In addition, the RHC component emissions from Io-C are seen in excellent detail; these observations, along with modulation lane measurements, give additional evidence that may suggest that both RHC and LHC emissions are coming from the same hemisphere source regions.

Observations of Io-B and Io-D emissions are clearly seen with the dual polarization LWA1 measurements. The Io-B data show characteristic arc and nested band structures, normal envelope and tail structures due to source geometry and beaming, and characteristic S-bursts that occur early in the Io-B events. The Io-D events are easily seen and analyzed with the LWA1 instrument. The Io-D events show characteristic LHC polarization and one event (Figure 7) shows narrow band structure.

The LWA1 instrument shows excellent fine structure in Jupiter's emission. Modulation lanes are clearly seen in both polarizations and drift rate measurements are consistent with earlier results. However, modulation lane measurements from one Io-A/Io-C event where both polarizations are observed simultaneously (Figure 12) might provide good constraints on the emission theory and growth mechanisms. More detailed analysis of additional Io-A/Io-C events are underway to further investigate the modulation lane details. Faraday fringes are also clearly seen in the LWA1 data and provide clues about the local conditions at the emission source, in the Io plasma torus, and the Earth's ionosphere.

Finally, and perhaps most interestingly, we have made excellent spectral and temporal measurements of S-bursts, N-events, and S-N events. First we have clearly detected S-bursts in the Io-D source, a measurement that is rare and will be useful to help understand the mechanism of S-burst emission. Drift rates of -12 MHz/s were measured for the Io-D region and are consistent with known drift rates from other Io-related sources. Several N-events are seen in our data in Io-A, Io-B, and Io-D events, but most interesting are the S-N events seen in an Io-B observation (Figures 14-15). These events display complex interaction where S-bursts appear to quench N-events, and N-events may trigger more S-bursts. These effects demonstrate that the emission mechanisms for the S-N events are similar and/or interacting, and that they are generated in the same spatial location. As mentioned previously, more observations of Io-D are being made in anticipation of further study of the S-bursts measured with the LWA1 instrument.

Acknowledgments. We thank the referees for a careful reading of the manuscript and helpful comments. We also wish to thank the staff of the Long Wavelength Array. Basic research in radio astronomy at the Naval Research Laboratory is supported by 6.1 Base funding. Construction of LWA1 was supported by the Office of Naval Research under Contract N00014-07-C- 0147. Support for operations and continuing development of LWA1 is provided by the National Science Foundation under grants AST-1139963 and AST-1139974 of the University Radio Observatories program. CAH acknowledges support from the Tennessee Space Grant Consortium. This research has been supported in part by JSPS KAKENHI Grant Number 25400480. JS (a student at Montgomery Blair High School) was supported by the Science and Engineering Apprenticeship Program (SEAP) at the Naval Research Laboratory. GBT acknowledges partial support for this work from NSF grant AST-1212162. Data used for this publication are available through request to the authors.

Notes

1. 1 Jy = 10^{-26} Watt m^{-2} Hz^{-1}
2. Radio Jupiter Pro software based on U. Florida probability tables
3. Examples can be found in the NDA catalog: http://typhon.obspm.fr/maser/SILFE

References

Alexander, J. K., Carr, T. D., Theiman, J. R., Schauble, J. J., & Riddle, A. C. 1981, *J. Geophys. Res.,* , 86, 8529

Alexander, J. K., & Desch, M. D. 1984, *J. Geophys. Res.,* , 89, no. 5, 2689

Arkypov, O. V. & Rucker, H. O. 2009, *Astron. Astrophys.,* , 496, 269

Barrow, C. H., Genova, F., & Desch, M. D. 1986, *Astron. Astrophys.,* , 165, 244

Bigg, E. K. 1964, Nature, 203, 1008

Boischot A., Rosolen, C., Aubier, M. G., Daigne, G., Genova, F. Leblanc Y., Lecacheux, A., De la Noe. J., & Moller-Pedersen, B., 1980, Icarus, 43, 399

Boischot, A., Lecacheux, A., Kaiser, M. L., et al. 1981, *J. Geophys. Res.,* , 86, 8213

Boudjada, M. Y., & Genova, F. 1991, Astronomy & Astrophysics, Supplement, 91, 453

Boudjada, M. Y., Rucker, H. O. & Ladreiter, P. H. 1995, *Astron. Astrophys.,* , 303, 255

Braude, S. I., Megn, A. V., Riabov, B. P., Sharykin, N. K., & Zhuk, I. N. 1978, Astrophysics and Space Sciences, 54, 3

Burke, B. F., & Franklin, K. L. 1955, *J. Geophys. Res.,* , 60, 213

Carr, T. D., Desch, M. D., & Alexander, J. K. 1983, Physics of the Jovian Magnetosphere, 226

Carr, T. D., & Reyes, F. 1999, *J. Geophys. Res.,* , 104, 25127

Clarke, J. T., Grodent, D., Cowley, S. W. H., et al. 2004, Jupiter. The Planet, Satellites and Magnetosphere, 639

Dowell, J. 2011, Long Wavelength Array Memo Series # 178, http://www.phys.unm.edu/∼lwa/memos

Dowell, J., Wood, D., Stovall, K., et al. 2012, Journal of Astronomical Instrumentation, 1, 1250006

Dulk, G. A. 1967, ICARUS, 7, 173

Dulk, G. A., Lecacheux, A., & Leblanc, Y. 1992, *Astron. Astrophys.,* , 253, 292

Dulk, G. A., Leblanc, Y., & Lecacheux, A. 1994, *Astron. Astrophys.,* , 286, 683

Ellingson, S., Liu, Q., and Craig, J. 2010, Long Wavelength Array Memo Series # 176, http://www.phys.unm.edu/∼lwa/memos

Ellingson, S. W., Taylor, G. B., Craig, J., et al. 2013, IEEE Transactions on Antennas and Propagation, 61, 2540

Flagg, R. S., Greenman, W. B., Reyes, F., & Carr, T. D. 1991, NASA STI/Recon Technical Report N, 91, 27047

Goldstein, M. L., & Thieman, J. R. 1981, *J. Geophys. Res.,* , 86, 8569

Gurnett, D. A., & Goertz, C. K. 1981, *J. Geophys. Res.,* , 86, 717

Hanasz, J., Panchenko, M., de Feraudy, H., Schreiber, R., & Mogilevsky, M. M. 2003, Journal of Geophysical Research (Space Physics), 108, 1408

Hess, S., Zarka, P., & Mottez, F. 2007, Planetary and Space Science, 55, 89

Hess, S., Cecconi, B., & Zarka, P. 2008, *Geophys. Res. Lett.,* , 35, 13107

Hess, S., Zarka, P., Mottez, F., & Ryabov, V. B. 2009, Planetary and Space Science, 57, 23

Hess, S. L. G., Echer, E., & Zarka, P. 2012, Planetary and Space Science, 70, 114

Hicks, B. C., Paravastu-Dalal, N., Stewart, K. P., et al. 2012, *Publ. A. S. P.,* , 124, 1090

Imai, K., Wang, L., & Carr, T. D. 1992, Geophys. Res. Lett., 19, 953

Imai, K., Wang, L., & Carr, T. D. 1997, *J. Geophys. Res.,* , 102, 7127

Imai, K., Clarke, T., Imai, M., Higgins, C. A., & Reyes, F. 2013, Magnetospheres of Outer Planets meeting, July 8-12, 2013, Athens, Greece

Kaiser, M. L., Zarka, P., Kurth, W. S., Hospodarsky, G. B., & Gurnett, D. A. 2000, *J. Geophys. Res.,* , 105, 16053

Leblanc, Y. 1981, *J. Geophys. Res.,* , 86, 8546

Lecacheux, A., Boischot, A., Boudjada, M. Y., & Dulk, G. A. 1991, *Astron. Astrophys.,* , 251, 339

Lecacheux, A., Kurth, W. S., & Manning R., 2001, in Planetary Radio Emissions V, edited by H. O. Rucker, M. L. Kaiser, and Y. Leblanc, Austrian Academy of Sciences Press, Vienna.

Litvinenko, G. V., Rucker, H. O., Vinogradov, V. V., Leitner, M., & Shaposhnikov, V. E. 2004, *Astron. Astrophys.,* , 426, 343

Litvinenko, G. V., Lecacheux, A., Rucker, H. O., Konovalenko, A. A., Ryabov, B. P., Taubenschuss, U., Vinogradov, V. V. & Shaposhnikov, V. E. 2009, Astron. and Astrophys., 493, no. 2, 651

Litvinenko, G., Zakharenko, V., Rucker, H., et al. 2010, European Planetary Science Congress 2010, 31

Melrose, D. B., Hewitt, R. G., & Dulk, G. A. 1984, *J. Geophys. Res.,* , 89, A2, 897

Obenberger, K. & Dowell, J. 2011, Long Wavelength Array Memo Series # 183, http://www.phys.unm.edu/∼lwa/memos

Ortega-Molina, A., & Daigne, G. 1984, *Astron. Astrophys.,* , 130, 301

Ortega-Molina, A., & Lecacheux, A. 1991, *J. Geophys. Res.,* , 96, 11441

Oya, M., Oya H., Ono, T., & Iizima, M. 2002, Earth, Moon, and Planets, 88, 187

Queinnec, J., & Zarka, P. 1998, *J. Geophys. Res.,* , 103, 26649

Ray, L. C., & Hess, S. 2008, Journal of Geophysical Research (Space Physics), 113, 11218

Riihimaa, J. J. 1985, Earth, Moon, and Planets, 32, 9

Riihimaa, J. J. 1990, Earth Moon and Planets, 48, 49

Riihimaa, J. J., & Carr, T. D. 1981, The Moon and the Planets, 25, 373

Riihimaa, J. J. 1968, Astronomical Journal, 73, 265

Rohlfs, K., & Wilson, T. L. 2004, Tools of Radio Astronomy, 4th rev. and enl. ed., by K. Rohlfs and T.L. Wilson. Berlin: Springer, 2004

Taylor, G. B., Ellingson, S. W., Kassim, N. E., et al. 2012, Journal of Astronomical Instrumentation , 1, 50004

Thieman, J. R., & Smith, A. G. 1979, *J. Geophys. Res.,* , 84, 2666

Treumann, R. A. 2006, Astron. Astrophy. Rev, 13, no. 4, 229

van Haarlem, M. P., Wise, M. W., Gunst, A. W., et al. 2013, *Astron. Astrophys.,* , 556, A2

Wilkinson, M. H. 1989, *J. Geophys. Res.,* , 94, 11777

Wu, C. S., & Lee, L. C. 1979, *Astrophys. J.,* , 230, 621

Zarka, P. 1988, Planetary radio emissions II; Proceedings of the Second International Workshop, Graz, Austria, Sept. 7-9, 1987 (A89-39951 17-91). Wien, Verlag der Oesterreichischen Akademie der Wissenschaften, 1988, p. 327-342., 327

Zarka, P. 1998, *J. Geophys. Res.,* , 103, 20159

Zarka, P., Farges, T., Ryabov, B. P., Abada-Simon, M., & Denis, L. 1996, *Geophys. Res. Lett.,* , 23, 125

Zarka, P., Queinnec, J., & Crary, F. J. 2001, Planetary and Space Science, 49, 1137

Corresponding author: T. E. Clarke, Naval Research Laboratory, Code 7213, 4555 Overlook Ave SW, Washington, DC 20375, USA. (tracy.clarke.ca@nrl.navy.mil)